Optical Materials: X 12 (2021) 100091

Contents lists available at ScienceDirect

Optical Materials: X

journal homepage: www.journals.elsevier.com/optical-materials-x

Invited Article

(INVITED) On the mechanism leading to afterglow in Gd_2O_2S:Pr

Cees Ronda [a,*], Andries Meijerink [b]

[a] Philips Research, High Tech Campus 11, 5656, AE Eindhoven, the Netherlands
[b] Debye Institute of Nanomaterials Science, Utrecht University, Princetonplein 1, 3584, CC Utrecht, the Netherlands

ARTICLE INFO

Keywords:
Gd2O2S:Pr3+
Afterglow
Scintillator
Computed tomography
Eu3+
Luminescence

ABSTRACT

The performance of scintillator materials and phosphors for x-ray imaging is adversely affected by afterglow, giving rise to ghost images and thus compromising image quality. Here, the afterglow of the well-known computed tomography (CT) phosphor Gd_2O_2S:Pr is investigated with time-delayed afterglow spectroscopy. It is shown that these afterglow spectra mainly show Eu^{3+} emission. This points to a mechanism, during excitation across the bandgap, in which holes are captured by Pr^{3+} ions, resulting in Pr^{4+} and electrons are captured by Eu^{3+} ions, creating Eu^{2+}. Afterglow is due to thermal excitation of electrons from the valence band to Pr^{4+} ions (detrapping of holes from Pr^{4+}), restoring Pr^{3+} ions. Capture of the resulting holes in the valence band by Eu^{2+} ions leads to excited Eu^{3+} ions that generate Eu^{3+} emission thus causing the undesired afterglow. Time delayed Eu^{3+} afterglow spectra are observed already for very low Eu^{3+} concentrations (<10 ppm). These observations provide insight in the dominant afterglow mechanism in $Gd_2O_2S:Pr^{3+}$ phosphors and allow to optimize the performance and improve the CT image quality by selection of starting materials with the lowest possible Eu^{3+} contamination levels to effectively reduce afterglow without loss of light yield.

1. Introduction

Computed Tomography (CT) is an important medical imaging modality [1]. In a CT examination, the attenuation of X-rays by the body of the patient is measured while the X-ray source and detector combination is rotating around the patient. The imaging procedure should take place in a very short time, as patient movements will reduce the image quality [1,2]. The rotation speed that can be applied is however limited by the decay time of the emitting ion in the CT phosphor and by afterglow. One speaks of afterglow when the time dependent intensity drop is slower than expected based on the decay time of the emitting ion.

Typically, the ceramic or single crystalline scintillators have a thickness in the order of a few mm. The scintillator elements are structured, using reflective layers, to optimize the light impinging on the photodiodes (Fig. 1). The size of the small elements in the scintillator ceramics is adjusted to the size of the photodiodes capturing the visible light emitted by the ceramic scintillator. In CT a number of different scintillating materials (that convert the energy of the impinging X-rays into visible light) are used, some of these are $CdWO_4$, $(Y,Gd)_2O_3$:Eu, garnet materials doped with Ce^{3+} (e.g. $(Y,Tb,Lu)_3Al_5O_{12}$:Ce) and also Gd_2O_2S:Pr [3,4]. $CdWO_4$ is a self-activated material, used as single crystalline material while the other three materials rely on emission from an activator and are used in ceramic form. In Table 1 some of the performance parameters of these CT phosphors are summarized. Both $(Y,Gd)_2O_3$:Eu and the garnet materials can be processed to transparency as the host material possesses cubic symmetry. Gd_2O_2S crystallizes in hexagonal symmetry and consequently only translucent material can be obtained. Advantages of Gd_2O_2S:Pr are the high stopping power of the host lattice (due to its high density: 7.34 g/cm^3) and the relatively high light yield (40000 photons/MeV excitation energy). Disadvantage is the relatively long afterglow. The afterglow in $Gd_2O_2S:Pr^{3+}$ has been extensively investigated but so far the origin remains elusive. Several studies have shown that the afterglow of Gd_2O_2S:Pr can be reduced by co-doping with minute amounts of Ce^{3+} or F^- ions, however at the cost of some light yield [3–7].

To improve the image quality that can be realized in CT-scanners, reducing afterglow of the $Gd_2O_2S:Pr^{3+}$ phosphor is essential. Here we investigate the origin of afterglow and in the course of the investigations, it became clear that subtle differences in trace levels of impurities are important in the mechanism leading to afterglow as significant changes in afterglow were found in scintillating ceramics produced from different starting materials. In this paper, we will focus on the spectroscopic characterization of Gd_2O_2S:Pr powders and will demonstrate that especially Eu^{3+} impurities already at ppm levels give

* Corresponding author.
E-mail addresses: cees.ronda@philips.com (C. Ronda), a.meijerink@uu.nl (A. Meijerink).

https://doi.org/10.1016/j.omx.2021.100091
Received 3 September 2021; Accepted 14 September 2021
Available online 2 October 2021

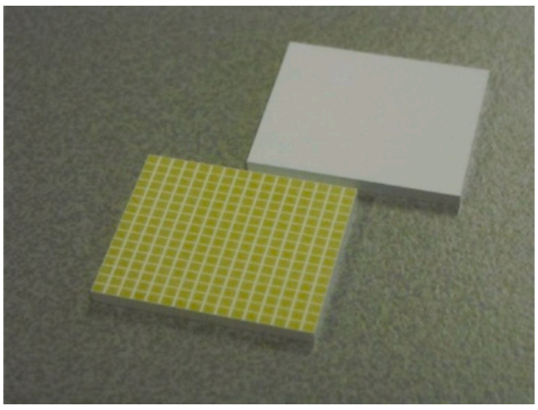

Fig. 1. Gd_2O_2S:Pr ceramic scintillator layer, with reflective layers. In the CT scanner the small squares are each connected with a light detector, monitoring the emission intensity from x-rays converted into light by the Gd_2O_2S:Pr^{3+} phosphor.

Table 1
Overview of performance parameters of a selection of commercially relevant scintillator materials for application in CT.

Material	Density (g/cm^3)	λ_{max} (nm)	Light yield (photons/MeV)	Decay time (ns)
$CdWO_4$	7.90	480	28000	10, 5000
$(Y,Gd)_2O_3$:Eu	5.91	611	19000	~10^6
Gd_2O_2S:Pr	7.34	510	40000	3000
$(Y,Tb,Lu)_5Al_5O_{12}$:Ce	>6.0	580	30000	60

rise to an increased afterglow that can be mitigated by selection of ultrapure starting materials with low Eu^{3+} levels.

2. Experimental

To investigate the origin of afterglow, high resolution emission spectra of Gd_2O_2S:Pr^{3+} microcrystalline powders were recorded using a Edinburgh FLS 920 spectrofluorometer, allowing for excitation over a wide wavelength range including 250 nm (4.85 eV, above the band gap of Gd_2O_2S which is 4.6 eV). Time-resolved emission spectra were recorded under pulsed (10 Hz, 10 ns pulse width) excitation over the bandgap with the fourth harmonic of a Spectra Physics Nd-YAG laser (266 nm). Emission spectra overlapping in time with the excitation pulse (direct emission) as well as emission spectra starting ~10 ms after the pulse (afterglow emission) were measured. The emission was collected with an optical fiber coupled to an Acton Research 0.25 m monochromator with a liquid nitrogen cooled Princeton Instruments CCD camera. By using a 150 lines/mm grating a wide spectral range could be detected. Typical integration times of 50 ms were selected to capture the afterglow emission spectrum within the time window of 100 ms in between excitation pulses.

3. Results and discussion

The emission spectra of Pr^{3+} in Gd_2O_2S are well known [8–10]. In Fig. 2 the emission spectrum of Gd_2O_2S:Pr^{3+} is shown for a typical material that is not intentionally doped with Eu^{3+} but does contain some Eu^{3+} impurities. Note that Eu^{3+} is a common impurity in Gd_2O_3 or other Gd-containing starting materials as neighboring lanthanides are the most abundant impurities based on the purification methods of lanthanides relying on differences in ionic radius. As Gd and Eu (element numbers 64 and 63) have similar ionic radii, relatively higher impurity levels of Eu (and also the other neighbor Tb, element 65) can be expected in Gd_2O_3 than in, for example, Lu_2O_3. The emission spectrum of

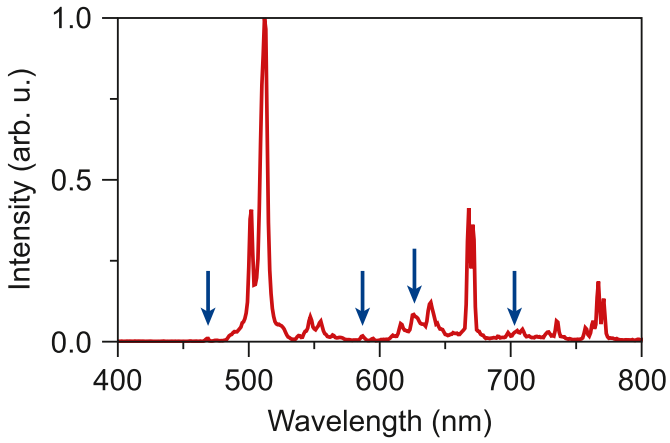

Fig. 2. Emission spectrum of Gd_2O_2S:Pr, without intentional doping with Eu^{3+}, excited with UV radiation at 250 nm at 300 K. The arrows indicate Eu^{3+} emission lines.

Gd_2O_2S:Pr^{3+} shows the characteristic strongest Pr^{3+} emission lines around 510 nm, weaker lines between 520 and 660 nm and stronger lines around 670 nm. The stronger emission lines correspond to $^3P_0$–$^3H_4$ emission (~510 nm) and $^3P_0$–$^3F_2$ emission (~670 nm). Weak emission lines that are observed under 250 nm (supra bandgap) excitation but not under ~450 nm direct excitation in the ^3P_J levels of Pr^{3+} are marked with blue arrows in Fig. 2. These weak lines are assigned to Eu^{3+} emission originating from the $^5D_2$ level (around 470 nm), $^5D_1$ level (around 530 nm) and $^5D_0$ level (around 585 and 620 nm).

To confirm that these weak emission lines originate from Eu^{3+} impurities, Gd_2O_2S:Pr^{3+} was synthesized with an additional 10 ppm Eu^{3+} (relative to Gd^{3+}), now intentionally added. The emission spectrum for this material under 250 nm excitation is shown in Fig. 3. One can clearly observe that the lines assigned to Eu^{3+} emission from the various ^5D_J levels are much more intense, confirming the assignment to Eu^{3+} emission and indicating very efficient energy transfer of the charge carriers/excitons created upon 250 nm excitation towards Eu^{3+} ions. Note that the Pr^{3+} concentration is significantly (100x) higher than the Eu^{3+} concentration with 0.1 mol% or 1000 mol ppm of Pr^{3+} vs. 10 ppm of Eu^{3+}. The relative intensity of the Pr^{3+} emission is less than 100x higher indicating that charge carriers or excitons created upon excitation over the bandgap are more efficiently captured by Eu^{3+}. The comparison also reveals that in the unintentionally doped material, the Eu^{3+} concentration is very small, significantly below 10 ppm and can be estimated to be around 2 ppm based on the approximately five times

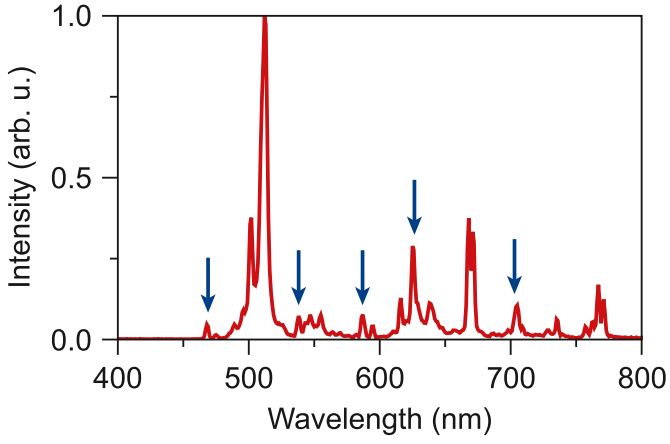

Fig. 3. Emission spectrum of Gd_2O_2S:Pr intentionally doped with Eu^{3+} (10 ppm), excited with UV radiation of 250 nm at 300 K. The arrows indicate Eu^{3+} emission lines.

lower relative intensity of the Eu^{3+} emission. Note the occurrence of Eu^{3+} emission lines not only from the $^5D_0$ but also from the $^5D_1$ and $^5D_2$ levels. Eu^{3+} emission originating from higher excited ^5D_J levels is observed only when Eu^{3+} concentrations are very low and in hosts with low phonon frequencies as cross-relaxation (for higher Eu-concentrations) and multi-phonon relaxation (for higher phonon energies) are known to quench emission from the higher energy $^5D_2$ and $^5D_1$ levels.

To investigate the origin of afterglow, Gd_2O_2S:Pr powder that is used in scintillating ceramics was excited with UV radiation of 266 nm that resulted from a pulsed and frequency quadrupled Nd:YAG laser. The photon energy (4.7 eV) is larger than the band gap of Gd_2O_2S (4.6 eV), so excitation takes place across the band gap, in this way mimicking X-ray excitation in the creation of free charge carriers. The time integrated emission spectrum was recorded for emission overlapping with the excitation pulse and also starting ~10 ms after the laser pulse and are shown in Figs. 4 and 5, respectively.

The time integrated spectrum with accumulation in a time window including the excitation pulse shows well-known Pr^{3+} emission lines. The time integrated afterglow spectrum with accumulation starting ~10 ms after the pulse is completely different, it rather shows Eu^{3+} emission and only a trace of Pr^{3+} emission at 515 nm. Gd_2O_2S:Pr powders with highly reduced Eu-content as selected for the production of scintillating ceramics did, if at all, hardly show Eu^{3+} emission when accumulation started after 10 ms. They rather showed very weak Pr^{3+} emission only, indicative of a much smaller afterglow.

The findings described above clearly shows that Eu^{3+} plays a pivotal role in the afterglow mechanism. We propose that after the optical excitation across the bandgap trapping of the free charge carriers created occurs by Pr^{3+} and Eu^{3+}. Pr^{3+} is converted into Pr^{4+}, and Eu^{3+} is converted into Eu^{2+}. Afterglow is due the reverse process, an electron from the valence band is thermally excited to Pr^{4+}, rendering Pr^{3+}. The resulting hole in the valence band is captured by Eu^{2+}, resulting in an excited Eu^{3+} ion that generates the observed Eu^{3+} emission. The steps are:

1. $Pr^{3+} + Eu^{3+} + h\nu_{exc} \rightarrow Pr^{4+} + Eu^{2+}$

2. $Pr^{4+} + Eu^{2+} + \Delta T \rightarrow Pr^{3+} + Eu^{3+}$ *

3. Eu^{3+} * $\rightarrow Eu^{3+} + h\nu_{em}$

The corresponding energy level diagram is given in Fig. 6. To validate the model proposed for the afterglow, the energies in this diagram have been taken from Refs. [11,12]. The thermal detrapping energy for a hole trapped by Pr^{4+} is ~0.4 eV which is consistent with slow thermal release of holes from Pr^{4+} to the valence band at room temperature.

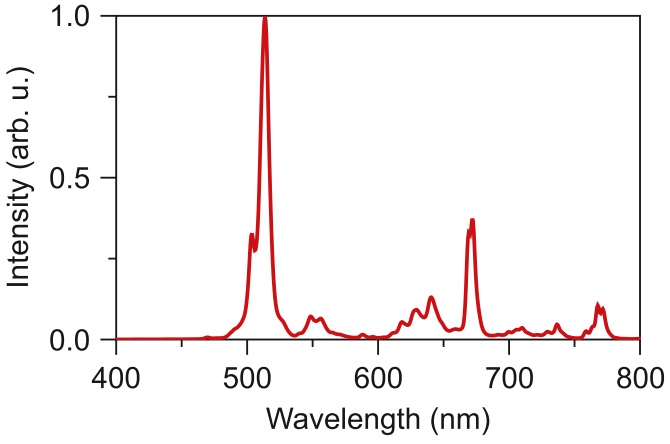

Fig. 4. Time integrated emission spectrum of Gd_2O_2S:Pr, excited at 266 nm over band gap with 10 ns 266 nm pulses of a quadrupled Nd-YAG laser for light accumulation of ~50 ms overlapping with the excitation pulse.

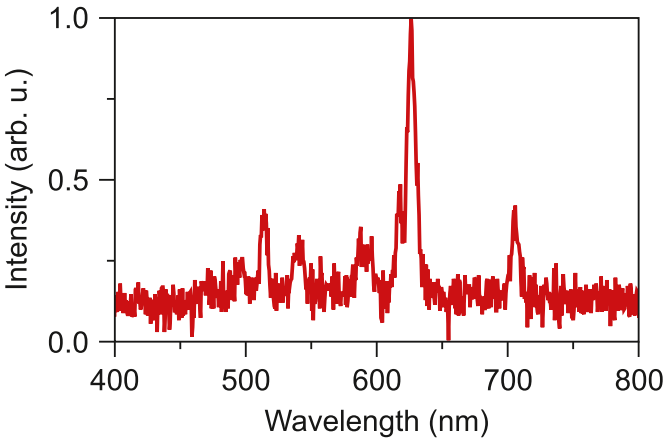

Fig. 5. Time integrated emission spectrum of Gd_2O_2S:Pr, excited at 266 nm over band gap with 10 ns 266 nm pulses of a quadrupled Nd-YAG laser for light accumulation of ~50 ms overlapping starting ~10 ms after the pulse.

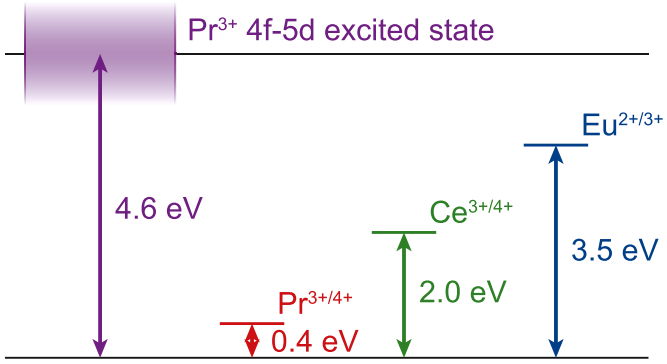

Fig. 6. Energy position of the ground states of Ce^{3+}, Pr^{3+} and Eu^{3+} in Gd_2O_2S (band gap 4.6 eV). The spectral position of the Pr^{3+} 4f-5fd position is also indicated. Adapted from Ref. [12].

Recombination of the valence band hole with Eu^{2+} produces Eu^{3+} in the excited ^5D_J states and the characteristic Eu^{3+} afterglow emission. Note also that the thermal trap depth of the electron trapped on Eu^{2+} in this band diagram is larger and thus Eu^{2+} is relatively stable, making it the recombination center which is consistent with the observation of Eu^{3+} emission afterglow. It is also interesting to note that a similar charge transfer mechanism is operative in the ion couple Ce^{3+} - Eu^{3+}, in which it leads to strong luminescence quenching as has been reported by Blasse [13].

The location of the energy levels in Fig. 6 can also explain the role of Ce^{3+} in reducing afterglow. As the ionization energy level of Ce^{3+} is located near the middle of the energy gap. In this manner Ce^{3+} competes with hole trapping by Pr^{3+} but does not release holes at room temperature. Recombination of a conduction band electron with Ce^{4+} results in Ce^{3+} in the excited 5d state, which is known to be non-luminescent in Gd_2O_2S. This mechanism explains the reduced afterglow and also the reduced light yield since Ce^{3+} does not emit in Gd_2O_2S resulting in some light loss [12]. For this reason, the Ce^{3+} concentration should be as low as possible, and the optimum concentration in turn, is determined by the Eu^{3+} concentration in Gd_2O_2S (see also [14]) and the content of cerium is to be chosen such that it is in excess of the content of europium with a ratio of Eu to Ce of 1:10 to 1:150.

4. Conclusions

The afterglow mechanism operative in Gd_2O_2S:Pr scintillators is investigated. It is shown that Eu^{3+} ions, present in trace amounts, play a

major role. Upon excitation across the bandgap (by x-rays or UV radiation) free charge carrier trapping causes Pr^{3+} to be oxidized to Pr^{4+} and Eu^{3+} to be reduced to Eu^{2+}. Thermal excitation at room temperature releases the hole trapped by Pr^{4+} and the resulting valence band hole is captured by Eu^{2+}, rendering excited Eu^{3+} and leading to Eu^{3+} afterglow. The present findings are consistent with earlier observations that afterglow can be reduced by addition of small amounts of Ce^{3+} (albeit at the expense of light yield). More importantly, it shows how reduction of afterglow without loss of light yield can be achieved by using ultrapure (low Eu^{3+} contamination levels) starting materials in the scintillator production process. This can help in improving the quality of images in computed tomography with $Gd_2O_2S:Pr^{3+}$ scintillators.

Declaration of competing interest

The authors declare that they have no known competing financial interests or personal relationships that could have appeared to influence the work reported in this paper.

Acknowledgement

We wish to express our gratitude to Dr. Freddy Rabouw for his help with the creation of the figures in this article.

References

[1] G. Blasse, B.C. Grabmaier, 'Luminescent Materials', Springer Verlag, Heidelberg, 1994, p. Chapter 8.
[2] J.G. Mainprize, M.J. Yaffe, Med. Phys. 25 (1998) 2440.
[3] B. C. Grabmaier, J. Lumin. 60&61 (1994) 967–970.
[4] C. Greskovich, S. Duclos, Annu. Rev. Mater. Sci. 27 (1997) 69–88.
[5] H. Yamada, A. Suzuki, Y. Uchida, M. Yoshida, H. Yamamoto, Y. Tsukuda, J. Electrochem. Soc. 136 (1989) 2713.
[6] R. Nakamura, N. Yamada, M. Ishii, Jap. J. Appl. Phys. 38 (1999) 6923.
[7] C.J. Michail, Sensors (2015) 874637.
[8] S. Blahuta, B. Viana, A. Bessière, E. Mattmann, B. LaCourse, Opt. Mater. 33 (2011) 1514–1518.
[9] G. Blasse, G.J. Dirksen, J. Solid State Chem. 73 (1988) 599.
[10] G. Blasse, A. Meijerink, Inorg. Chim. Acta. 160 (1989) 29–31.
[11] H. Luo, A.J.J. Bos, P. Dorenbos, J. Phys. Chem. C 121 (2017) 8760–8769.
[12] P.A. Rodnyi, Opt Spectrosc. 107 (2009) 270.
[13] G. Blasse, Phys. Status Solidi 75 (1983) K41.
[14] C.R. Ronda, G. Zeitler, D. Waedow, H. Wieczoreck, H. Schreinemacher, 'Procedure to obtain Gd_2O_2S: Pr for CT with a very short afterglow', US patent 8057702B2 (2006).